mission 0.634/0.756, 51123 reflections collected, 11056 independent reflections ($R_{int} = 0.056$), 8979 observed reflections with $I > 2\sigma(I)$, 308 parameters, max residual electron density 1.544 e Å^{-3}, $R_1 = 0.040$, $wR_2 = 0.092$; K, Se, Mo, Cl refined anisotropically. $K_2[Se^{IV}Mo_6O_{21}(O_2CCHCH_3NH_3)_3]\cdot 4.5\,H_2O$: $0.30 \times 0.20 \times 0.10$ mm^3, orthorhombic, space group $P2_12_12_1$, $Z = 4$, $T = 293(2)$ K, $a = 11.2576(16)$, $b = 16.655(2)$, $c = 19.285(3)$ Å, $V = 3616.0(9)$ Å^3, $2\theta_{max} = 56.6°$, $\rho_{calcd} = 2.587$ Mg m^{-3}, $\mu = 3.364$ mm^{-1}, min/max transmission 0.375/0.621, 40856 reflections collected, 8833 independent reflections ($R_{int} = 0.067$), 7967 observed reflections with $I > 2\sigma(I)$, 267 parameters, max residual electron density 1.316 e Å^{-3}, $R_1 = 0.038$, $wR_2 = 0.097$; K, Se, Mo refined anisotropically. $K_2[Te^{IV}Mo_6O_{21}(O_2CCH_2NH_3)_3]\cdot 8\,H_2O$: $0.30 \times 0.14 \times 0.10$ mm^3, orthorhombic, space group $Pnma$, $Z = 4$, $T = 173(2)$ K, $a = 13.9561(18)$, $b = 20.805(3)$, $c = 12.3770(16)$ Å, $V = 3593.7(8)$ Å^3, $2\theta_{max} = 56.6°$, $\rho_{calcd} = 2.709$ Mg m^{-3}, $\mu = 3.176$ mm^{-1}, min/max transmission 0.596/0.719, 39150 reflections collected, 4557 independent reflections ($R_{int} = 0.051$), 4156 observed reflections with $I > 2\sigma(I)$, 144 parameters, max residual electron density 1.663 e Å^{-3}, $R_1 = 0.057$, $wR_2 = 0.132$; K, Te, Mo refined anisotropically. $K(H_3N(CH_2)_2COOH)[Te^{IV}Mo_6O_{21}(O_2C(CH_2)_2NH_3)_3]\cdot 3\,H_2O$: $0.20 \times 0.16 \times 0.08$ mm^3, monoclinic, space group $P2_1/c$, $Z = 4$, $T = 173(2)$ K, $a = 10.7020(14)$, $b = 20.831(3)$, $c = 16.771(2)$ Å, $\beta = 97.527(2)$, $V = 3706.6(9)$ Å^3, $2\theta_{max} = 56.7°$, $\rho_{calcd} = 2.657$ Mg m^{-3}, $\mu = 2.966$ mm^{-1}, min/max transmission 0.634/0.704, 42108 reflections collected, 9096 independent reflections ($R_{int} = 0.062$), 6903 observed reflections with $I > 2\sigma(I)$, 265 parameters, max residual electron density 1.660 e Å^{-3}, $R_1 = 0.043$, $wR_2 = 0.090$; K, Te, Mo refined anisotropically. $Cs_2[Te^{IV}Mo_6O_{21}(O_2C(CH_2)_3NH_3)_3]\cdot 5.25\,H_2O$: $0.18 \times 0.16 \times 0.10$ mm^3, monoclinic, space group $P2_1/n$, $Z = 4$, $T = 293(2)$ K, $a = 11.3740(16)$, $b = 22.231(3)$, $c = 16.887(2)$ Å, $\beta = 102.535(2)$, $V = 4168.3(10)$ Å^3, $2\theta_{max} = 56.7°$, $\rho_{calcd} = 2.697$ Mg m^{-3}, $\mu = 4.259$ mm^{-1}, min/max transmission 0.507/0.612, 46889 reflections collected, 10230 independent reflections ($R_{int} = 0.051$), 8117 observed reflections with $I > 2\sigma(I)$, 282 parameters, max residual electron density 1.471 e Å^{-3}, $R_1 = 0.039$, $wR_2 = 0.086$; Cs, Te, Mo refined anisotropically. $K_2Na[As^{III}Mo_6O_{21}(O_2CCH_2NH_3)_3]\cdot 6\,H_2O\cdot 0.5\,Cl$: $0.22 \times 0.06 \times 0.04$ mm^3, monoclinic, space group $P2_1$, $Z = 2$, $T = 173(2)$ K, $a = 11.7166(17)$, $b = 13.753(2)$, $c = 11.8154(17)$ Å, $\beta = 115.121(2)$, $V = 1723.8(4)$ Å^3, $2\theta_{max} = 56.8°$, $\rho_{calcd} = 2.749$ Mg m^{-3}, $\mu = 3.479$ mm^{-1}, min/max transmission 0.636/0.856, 20056 reflections collected, 7708 independent reflections ($R_{int} = 0.076$), 6330 observed reflections with $I > 2\sigma(I)$, 277 parameters, max residual electron density 1.320 e Å^{-3}, $R_1 = 0.050$, $wR_2 = 0.102$; K, Na, As, Mo, Cl refined anisotropically. $K_{2.5}Na[Sb^{III}Mo_6O_{21}(O_2CCH_2NH_3)_3]\cdot 6\,H_2O\cdot 0.5\,Cl$: $0.10 \times 0.08 \times 0.02$ mm^3, monoclinic, space group $P2_1$, $Z = 2$, $T = 173(2)$ K, $a = 11.7166(17)$, $b = 13.753(2)$, $c = 11.8154(17)$ Å, $\beta = 115.121(2)$, $V = 1723.8(4)$ Å^3, $2\theta_{max} = 56.8°$, $\rho_{calcd} = 2.877$ Mg m^{-3}, $\mu = 3.354$ mm^{-1}, min/max transmission 0.705/0.819, 20076 reflections collected, 8344 independent reflections ($R_{int} = 0.068$), 6870 observed reflections with $I > 2\sigma(I)$, 277 parameters, max residual electron density 1.682 e Å^{-3}, $R_1 = 0.051$, $wR_2 = 0.097$. K, Na, Sb, Mo, Cl refined anisotropically. CCDC-190479–190487 contains the supplementary crystallographic data for this paper. These data can be obtained free of charge via www.ccdc.cam.ac.uk/conts/retrieving.html (or from the Cambridge Crystallographic Data Centre, 12, Union Road, Cambridge CB2 1EZ, UK; fax: (+44) 1223-336-033; or deposit@ccdc.cam.ac.uk).

[24] I. D. Brown, D. Altermatt, *Acta Crystallogr. Sect. B* **1985**, *41*, 244–247.
[25] G. M. Sheldrick, *Acta Crystallogr. Sect. A* **1990**, *46*, 467–473; SHELXS-97, Structure Determination Software Programs, SAINT, Version 4.050, **1996** and *SADABS*, Bruker Analytical X-ray Instruments, Madison, Wisconsin, USA, **1997**.

Preparation and Characterization of a Model Bimetallic Catalyst: Co–Pd Nanoparticles Supported on Al_2O_3**

Michael Heemeier, Anders F. Carlsson, Matthias Naschitzki, Martin Schmal, Marcus Bäumer,* and Hans-Joachim Freund

The development of well-defined model systems is an important precondition for studies aimed at an understanding of catalytic mechanisms at the microscopic level. In this context, the bridging of the so-called "materials gap", that is the adjustment of the model systems to the complexity of real catalysts, is essential. Accordingly, in the case of supported metal catalysts, the focus has shifted from single crystals, which were studied in the beginning to understand adsorption and reaction on extended surfaces, to metal particles deposited on oxide supports.[1,2] The latter systems allow the investigation of particle size effects as well as metal–support interactions, that is factors that can equally be decisive for the overall catalytic performance. Although some progress has been achieved in recent years in this field, the question remains how model systems for more complex systems can be prepared in a defined and reproducible manner.

Herein, we deal with this question for bimetallic catalysts. Such materials represent a highly interesting class of catalysts because one metal can tune and/or modify the catalytic properties of the other metal as the result of both ligand (electronic) and ensemble (structural) effects.[3] Bimetallic Pd–Co particles, for example, have shown improved selectivity over pure Co particles in Fischer–Tropsch reactions.[4–8] Since the conversion of natural resources into syngas ($CO + H_2$) and then to clean fuels through the Fischer–Tropsch reaction will likely become evermore important with changing supplies and environmental concerns,[9] a detailed understanding of such effects by means of suitable model systems is needed.

Our approach is based on metal vapor deposition on a suitable oxide support under ultrahigh vacuum (UHV) conditions. For the present study, a thin alumina film grown on a metallic NiAl(110) substrate was used,[10] which enabled us to apply scanning tunneling microscopy (STM) as well as temperature-programmed desorption (TPD) for the charac-

[*] Priv.-Doz. Dr. M. Bäumer, M. Heemeier, Dr. A. F. Carlsson, M. Naschitzki, Prof. Dr. H.-J. Freund
Fritz-Haber-Institut der Max-Planck-Gesellschaft
Abteilung Chemische Physik
Faradayweg 4–6, 14195 Berlin (Germany)
Fax: (+49) 30-8413-4101
E-mail: baeumer@fhi-berlin.mpg.de
Prof. Dr. M. Schmal
NUCAT-COPPE
Federal University of Rio de Janeiro (Brazil)

[**] This work was supported by the Max-Planck Society and the Deutsche Forschungsgemeinschaft. A.F.C. thanks the Alexander von Humboldt Foundation for a fellowship. We thank Prof. V. Matolin (Prague), Prof. J. Nørskov (Lynbgy), and Dr. T. Risse (Fritz-Haber-Institut, Berlin) for valuable discussions, and K. H. Hansen (group of Prof. Besenbacher, Åarhus) for experimental contributions at the beginning of the project.

  0044-8249/02/4121-4073 $ 20.00+.50/0

terization of the samples. On this film, nanometer-sized Pd–Co particles were generated by sequentially depositing the two constituents onto this support. Inspired by earlier work by Henry and coworkers,[11,12] different structures and compositions of the particles were obtained in a controllable way by taking advantage of the different nucleation and growth properties of the two metals.

This is demonstrated in Figure 1 by STM images taken after depositing Pd and Co alone and together on the film. In the case of pure Pd, the data show that the majority of Pd particles nucleate and grow at line defects of the support. As discussed in detail elsewhere, these line defects, which appear as protruding lines in the differentiated part of the image (upper left corner), are antiphase and reflection domain boundaries of the alumina film.[13] Another point to note is the regular shape of the aggregates which suggests that they have a crystalline structure. Closer inspection shows that the sides and top are mainly formed by (111) faces.[14] In contrast, pure Co preferentially nucleates at point defects on the alumina film.[15,16] As can be inferred from the corresponding STM image, this results in both a higher particle density and a more homogeneous particle distribution on the surface. Unlike for Pd, there are no indications of crystalline order of the Co aggregates.

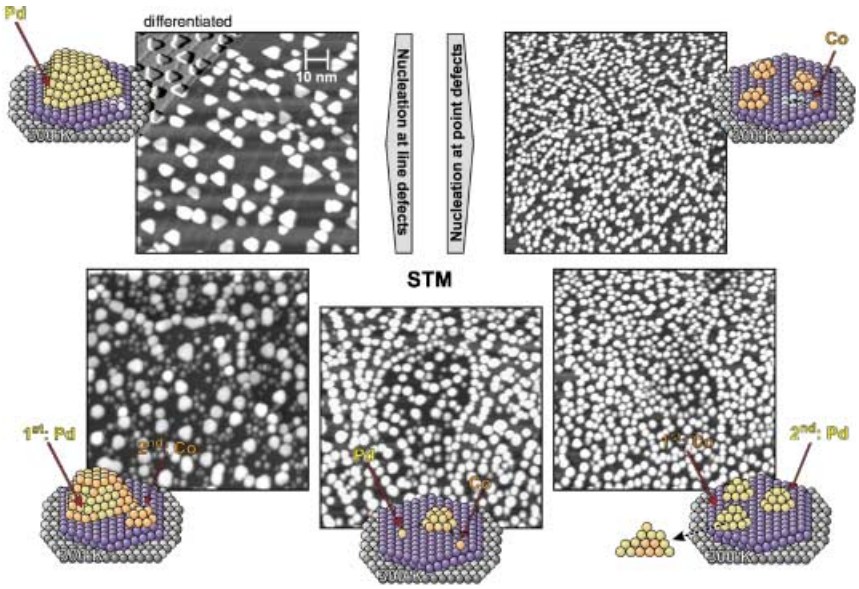

Figure 1. STM images (100 nm × 100 nm) taken after depositing 2 Å Pd and 2 Å Co alone (top row) and together (bottom row) onto a thin alumina film at 300 K. In the latter case the metals have either been deposited sequentially (left: 1st Pd, 2nd Co; right: 1st Co, 2nd Pd) or simultaneously (middle). The ball models schematically show the structure of the systems investigated: gray: NiAl substrate; blue: Al_2O_3 film; light blue: defects of the alumina film; yellow: Pd atoms; orange: Co atoms.

Let us now assume that Pd is deposited on a surface already covered by Co particles. Owing to the higher mobility of Pd on the surface, it will be trapped at Co particles before reaching the line defects. The STM image presented in Figure 1 essentially corroborates this expectation. The arrangement of particles found for this sequence strongly resembles that for pure Co, thus suggesting particles with a Co core and a Pd shell. If, on the other hand, Pd is deposited first, the less mobile Co atoms should partly cover the Pd crystallites and partly nucleate between them. The STM image indeed shows triangular and hexagonal crystallites as well as the large number of new small clusters between them.

In addition to these sequential deposition experiments, we also performed a codeposition experiment. The corresponding STM image (Figure 1, lower row, center) reveals a situation intermediate to the results of the sequential preparation. As the structure of these particles (alloy particles or core/shell structures) is presently unclear, they will not be considered in the following.

To verify the surface composition of our model systems, we performed temperature-programmed desorption experiments using CO as a probe molecule. In this context, it is important to know that CO prefers *different adsorption sites* on the two metals. On Pd, CO is bound preferentially to threefold hollow sites, followed by bridge sites, and finally atop sites.[17,18] On Co the order is reversed: CO is bound preferentially to atop sites, followed by more highly coordinated sites.[19,20]

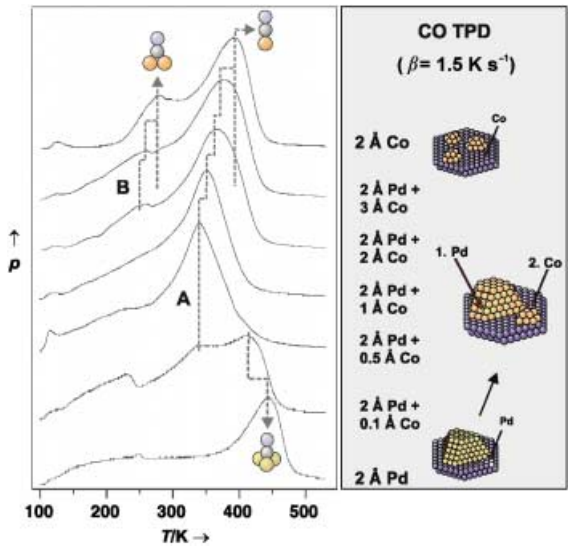

Figure 2. Temperature-programmed desorption spectra of CO from bimetallic Pd–Co particles supported on Al_2O_3/NiAl(110). The particles were prepared by depositing 2 Å Pd (1 Å Pd $\hat{=}$ 6.8×10^{14} cm^{-2}) first and various amounts of Co subsequently. The spectra for pure Pd and Co particles are also shown for reference. An exposure of 20 L CO (1 L $\hat{=}$ 10^{-6} Torr) was given at 100 K prior to TPD. The heating rate was 1.5 K s^{-1}. Color code for the models see Figure 1.

Two series of TPD spectra from the bimetallic particles are plotted in Figure 2 and 3 for the sequence 1st Pd/2nd Co and 1st Co/2nd Pd, respectively. The bottom spectrum of Figure 2 and the top spectrum of Figure 3 shows the desorption of CO from pure Pd. The main peak at about 450 K is due to desorption from threefold hollow sites, in agreement with data from Pd(111) single-crystal surfaces[18] and with an IR spectroscopic study on metal particles.[21] The broad shoulder

  0044-8249/02/4121-4074 $ 20.00+.50/0

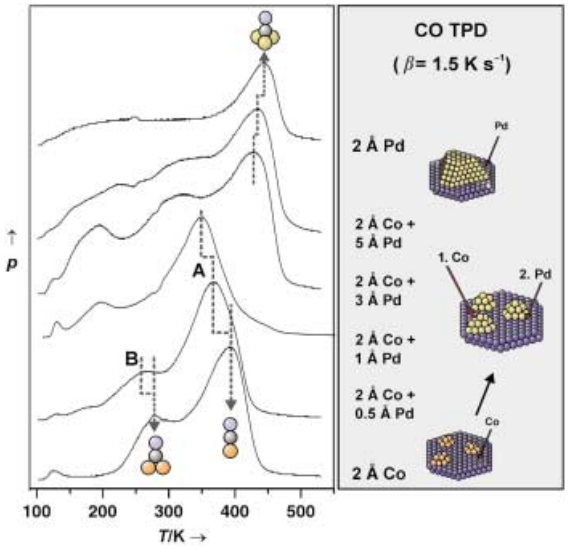

Figure 3. Temperature-programmed desorption spectra of CO from bimetallic Pd–Co particles supported on Al_2O_3/NiAl(110). The particles were prepared by depositing 2 Å Co (1 Å Co $\hat{=}$ 9.0×10^{14} cm^{-2}) first and various amounts of Pd subsequently. The spectra for pure Pd and Co particles are also shown for reference. An exposure of 20 L CO (1 L $\hat{=}$ 10^{-6} Torr s) was given at 100 K prior to TPD. The heating rate was 1.5 K s^{-1}. Color code for the models see Figure 1.

at lower temperatures most likely results from the gradual depopulation of bridge and atop sites. For pure Co particles (top spectrum of Figure 2 and bottom spectrum of Figure 3), we assign the desorption at about 390 K to atop sites and the shoulder at about 280 K to bridge sites, in analogy to literature data from single-crystal surfaces.[20]

Turning to the bimetallic systems, for the deposition order 1st Pd/2nd Co it is interesting to note that small amounts of Co deposited onto a film covered by Pd particles result in large changes in the TPD spectrum. At the beginning of the deposition series, a significant lowering of the desorption temperature from Pd threefold hollow sites can be detected (ca. 25 K). Concomitantly, a new feature evolves at about 350 K, which becomes dominant with increasing Co coverage and finally suppresses the desorption from the Pd hollow site.

In principle, two effects can be responsible for the different adsorption and desorption behavior of an alloy as compared to the pure metals: electronic and structural effects.[22,23] The first effect, also called ligand effect, is encountered if the interaction between an adsorbate and a particular adsorption site is modified by a second metal surrounding that site. Since bimetallic bonding generally weakens the strength of the Pd–CO bond,[23] the downshift of the desorption maximum in the Pd spectrum can be readily explained by a ligand effect of Co covering the Pd crystallites. The second effect, called ensemble effect, is relevant only for highly coordinated sites, that is bridge or hollow sites. It is effective if one of the atoms constituting such a site is exchanged by the second metal so that the site is eliminated. As threefold hollow sites should be strongly affected by this effect, the early suppression of the corresponding peak in the Pd spectrum is not surprising.

With increasing Co coverage (Figure 2), the peak at 350 K shifts to higher temperatures until, at very high Co coverages, the desorption spectrum resembles that of pure Co. It is therefore tempting to assign the peak, labeled **A** in the spectra (Figure 2), to the desorption of terminally bonded CO from Co atoms on the Pd crystallites. The shift can be explained by a decreasing ligand effect of Pd as the Co coverage increases. Also note the peak, labeled **B**, that points to Co bridge sites appearing later in the series due to the ensemble effect expected in this case.

So far only desorption from the Co-covered Pd crystallites has been considered. In the intermediate coverage regime, however, the broad desorption maximum with a clear contribution (shoulder) at higher temperatures reveals that, according to STM images (Figure 1), the small Co particles that form between the Pd crystallites are also detectable in the TPD spectra.

For the deposition order 1st Co, 2nd Pd the TPD experiments (Figure 3) corroborate the structure inferred from the STM results as well. Here, a new desorption peak from CO atop sites evolves at lower temperature (**A**), which can be assigned to Co particles partly covered by Pd. The shoulder at the original desorption temperature still visible in the first spectrum of the series apparently results from areas on the particles not covered at this stage. The shift of the maximum to lower temperatures induced by Pd can again be understood in terms of the ligand effect discussed above. As the Pd coverage increases and its electronic influence becomes stronger, the desorption shifts to even lower temperatures and the desorption from pure Co sites vanishes.

Finally, when a Pd shell completely covering the Co cores is formed, desorption from Pd threefold hollow sites is detected in the spectra. At a first glance, it might be surprising that relatively large amounts of Pd are needed to observe this site. Two reasons, however, can be responsible for that: 1) the strong ensemble effect expected for this site and 2) the smaller and less ordered particles as compared to the other deposition order (cf. Figure 1) which possibly offer less intact threefold hollow sites.

In conclusion, we have presented a method to prepare oxide-supported bimetallic Pd–Co nanoparticles by metal vapor deposition. By taking advantage of nucleation and growth processes on the surface, particles of different structure and composition can be obtained. CO TPD experiments corroborate the structures suggested by STM, revealing that both ensemble and ligand effects change the adsorption properties of these bimetallic model catalysts.

Experimental Section

The UHV system used in this study has been described in detail elsewhere.[24] Briefly, it consists of a commercially built analysis chamber (Omicron) with an AFM/STM stage, as well as X-ray photoelectron spectroscopy (XPS) and low-energy electron diffraction (LEED) capabilities. Coupled to the analysis chamber by a transfer system is a preparation chamber containing Pd and Co metal evaporators, and facilities for sputtering, gas dosing, and TPD measurements. The flux of the metal evaporators was calibrated both with a quartz microbalance in a different chamber and checked by STM in the analysis chamber. To quantify the amount of material deposited, the nominal film thickness as measured by the microbalance is used in this article. The NiAl(110) crystal was cleaned by cycles of Ar^+ sputtering, and an Al_2O_3 film was prepared by previously described methods.[10,13]

Before the TPD measurements, the sample was given a directed dose of CO at 100 K and then placed less than 1 mm away from the differentially

  0044-8249/02/4121-4075 $ 20.00+.50/0

pumped cap of the quadropole mass spectrometer. The sample was heated by radiation from a tungsten filament mounted directly behind it. A linear temperature ramp for TPD was programmed with a controller and power supply from Schlichting Physikalische Instrumente. The spectra were obtained by recording the temperature and the partial pressures of the species desorbing from the surface during such a ramp. Blank measurements from the oxide film without deposited metal particles showed desorption of small amounts of masses 2, 16, 18, 28, 32, and 44 below 150 K resulting from desorption from the heating filament (CO does not adsorb on the clean alumina film above 90 K[13]); these signals were at least an order of magnitude smaller than those from the metal particles.

Received: April 30, 2002 [Z19203]

[1] *Advances in Catalysis, Vol. 45* (Eds.: B. C. Gates, H. Knözinger), Academic Press, San Diego, **2000**.

[2] *Frontiers in Surface and Interface Science* (Eds.: C. B. Duke, E. W. Plummer), Elsevier, Amsterdam, **2002**.

[3] J. H. Sinfelt, *Bimetallic Catalysts*, Wiley, New York, **1983**.

[4] H. Idriss, C. Diagne, J. P. Hindermann, A. Kinnemann, M. A. Barteau in *Proceedings, 10th International Congress on Catalysis, Budapest, 1992, Vol. Part C* (Eds.: L. Guczi, F. Solymosi, P. Tetenyi), Elsevier, Budapest, **1992**, p. 2119.

[5] M. P. Kapoor, A. L. Lapidus, A. Y. Krylova, *Proceedings, 10th International Congress on Catalysis, Budapest, 1992, Vol. Part C* (Eds.: L. Guczi, F. Solymosi, P. Tetenyi), Elsevier, Budapest, **1992**, p. 2741.

[6] W. Juszczyk, Z. Karpinski, D. Lomot, J. Pielaszek, Z. Paal, A. Y. Stakheev, *J. Catal.* **1993**, *142*, 617.

[7] F. B. Noronha, M. Schmal, C. Nicot, B. Moraweck, R. Frety, *J. Catal.* **1997**, *168*, 42.

[8] S. Bischoff, A. Weigt, K. Fujimoto, B. Lücke, *J. Mol. Catal. A* **1995**, *95*, 259.

[9] K. Weissermel, H.-J. Arpe, *Industrial Organic Chemistry*, 3rd ed., VCH, Weinheim, **1997**.

[10] R. M. Jaeger, H. Kuhlenbeck, H.-J. Freund, M. Wuttig, W. Hoffmann, R. Franchy, H. Ibach, *Surf. Sci.* **1991**, *259*, 235.

[11] F. Gimenez, C. Chapon, C. R. Henry, *New J. Chem.* **1998**, *22*, 1289.

[12] S. Giorgio, C. Chapon, C. R. Henry in *Metal Clusters in Chemistry* (Eds.: P. Braunstein, L. A. Oro, P. R. Raithby), Wiley-VCH, Weinheim, **1999**, p. 1194.

[13] M. Frank, M. Bäumer, *Phys. Chem. Chem. Phys.* **2000**, *2*, 3723.

[14] K. H. Hansen, T. Worren, S. Stempel, E. Laegsgaard, M. Bäumer, H.-J. Freund, F. Besenbacher, I. Stensgaard, *Phys. Rev. Lett.* **1999**, *83*, 4120.

[15] T. Hill, M. Mozaffari-Afshar, J. Schmidt, T. Risse, S. Stempel, M. Heemeier, H.-J. Freund, *Chem. Phys. Lett.* **1998**, *292*, 524.

[16] M. Bäumer, M. Frank, M. Heemeier, R. Kühnemuth, S. Stempel, H.-J. Freund, *Surf. Sci.* **2000**, *454-456*, 957.

[17] T. Giessel, O. Schaff, C. J. Hirschmugl, V. Fernandez, K. M. Schindler, A. Theobald, S. Bao, R. Lindsay, W. Berndt, A. M. Bradshaw, D. Baddleley, A. F. Lee, R. M. Lambert, D. P. Woodruff, *Surf. Sci.* **1998**, *406*, 90.

[18] X. Guo, J. T. Yates, Jr., *J. Chem. Phys.* **1989**, *90*, 6761.

[19] J. Lahtinen, J. Vaari, K. Kauraala, E. A. Soares, M. A. Van Hove, *Surf. Sci.* **2000**, *448*, 269.

[20] J. Lahtinen, J. Vaari, K. Kauraala, *Surf. Sci.* **1998**, *418*, 502.

[21] K. Wolter, O. Seiferth, H. Kuhlenbeck, M. Bäumer, H.-J. Freund, *Surf. Sci.* **1998**, *399*, 190.

[22] C. T. Campbell, *Annu. Rev. Phys. Chem.* **1990**, *41*, 775.

[23] J. A. Rodriguez, *Surf. Sci. Rep.* **1996**, *24*, 223.

[24] S. Stempel, Ph.D. thesis, Freie Universität, Berlin, **1998**.

  0044-8249/02/4121-4076 $ 20.00+.50/0